Check for updates

# Aluminyl derived ethene functionalization with heteroallenes, leading to an intramolecular ligand rearrangement†

Andrea O'Reilly, [ID] [a] Michael G. Gardiner, [ID] [b] Claire L. McMullin, [ID] *[c] J. Robin Fulton [ID] *[a] and Martyn P. Coles [ID] *[a]

The aluminacyclopropane K[Al(NON)(η-$C_2H_4$)] ([NON]$^{2-}$ = [O(SiMe$_2$-NDipp)$_2$]$^{2-}$, Dipp = 2,6-iPr$_2$C$_6$H$_3$) reacts with $CO_2$ and iPrN=C=NiPr to afford ring-expanded products of C–C bond formation. The latter system undergoes a 1,3-silyl retro-Brook rearrangement of the NON-group, to afford the [NNO]$^{2-}$ ligand ([NNO]$^{2-}$ = [N(Dipp)SiMe$_2$N-(Dipp)SiMe$_2$O]$^{2-}$). The mechanism of transformation was examined by density functional theory (DFT).

A defining goal in applied inorganic chemistry is the effective conversion of low-cost chemical feedstocks into value-added chemicals. Much of this research is focused on the combination of small organic molecules in the coordination sphere of an s- or p-block element to generate more complex molecules, relying on activation and subsequent bond forming/breaking processes of the substrates. This area has traditionally been dominated by transition-metals, although select main group metal complexes are emerging as viable alternatives,[1] with justifications for this research often citing the cost advantage of using earth abundant elements in these transformations.

The ready availability and economic accessibility of aluminium has led to the chemistry of this element being prominent in this field, with a fertile area involving low-valent Al(I) and Al(II) species.[2] In 2018, a new class of anionic Al(I) complex containing nucleophilic aluminyl anions was introduced.[3] These compounds have already demonstrated many examples of bond-breaking and bond-forming reactions initiated by the electron rich Al(I) centre, with examples of C–C bond formation featuring prominently in this research.

Acrylic acid (propenoic acid) is an important commodity chemical with a global market volume of approximately 8 million metric tonnes in 2022.[4] Processes used in the production of acrylates include the hydroxy-carbonylation of alkynes (Reppe chemistry)[5] and the oxidation of propene (Fig. 1).[6] An attractive alternative (that also helps to mitigate problems associated with greenhouse gases) involves the direct combination of $CO_2$ with alkenes.[7] A key step in this process is the C–C bond formation between the two substrates and, although endergonic under normal experimental conditions,[8] a series of systems based on d-block metals Ti,[9] Zr,[10] V,[11] Mo and W,[12] Fe,[13] Ru,[14] Rh,[15] Ni,[16] and Pd[17] promote this reaction. However, examples of $CO_2$/alkene coupling at main group metal centres are limited to matrix isolation experiments involving condensates of Mg atoms with $C_2H_4$/$CO_2$.[18]

Previous work has shown that the Al(I) compound Al(BDI) (BDI = [HC(CMeNDipp)$_2$]$^{2-}$) reacts reversibly with alkenes to generate the corresponding aluminacyclopropane species.[19] Although the products contain "activated" alkene bonds, reactivity is limited to the reversible insertion of CO into an Al–C
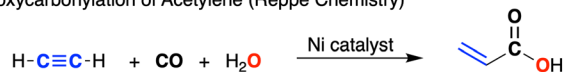
$^a$ *School of Chemical and Physical Sciences, Victoria University of Wellington, PO Box 600, Wellington 6012, New Zealand. E-mail: martyn.coles@vuw.ac.nz, j.robin.fulton@vuw.ac.nz*

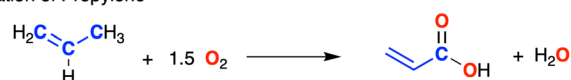$^b$ *Research School of Chemistry, The Australian National University, Canberra, ACT 2601, Australia*

$^c$ *Department of Chemistry, University of Bath, Bath, BA2 7AY, UK. E-mail: cm2025@bath.ac.uk*

Fig. 1 Methods for the production of acrylic acid.
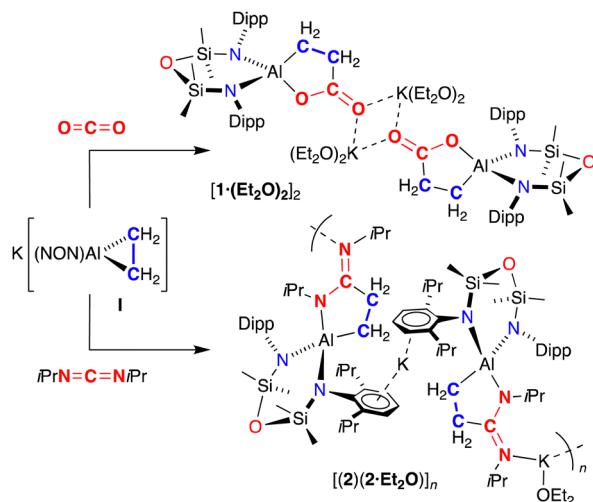
**Scheme 1** Synthesis of **1** and **2**.

bond of the aluminacyclopropane derived from norbornene.[20] This area has been extended to anionic aluminacyclopropane analogues derived from potassium aluminyl compounds,[21] and we have shown that the potassium aluminyl K[Al(NON)][22] reacts with ethene to form K[Al(NON)($\eta$-$C_2H_4$)] (**I**).[23] Reaction of **I** with CO under ambient conditions afforded the isolable CO insertion product, which underwent a thermal rearrangement to afford the propan-1,3-diyl-$\kappa^2C$-1-one containing product. In this study we demonstrate C–C bond forming reactions between an aluminacyclopropane and heteroallenes. In addition, we have studied an unusual ligand rearrangement of the normally innocent NON-ligand.

The reaction of aluminacyclopropane **I** with $^{13}CO_2$ proceeds under ambient conditions to form a new product, **1** (Scheme 1). $^1H$ NMR spectroscopy of **1** shows a non-symmetrical product in which the high field singlet in **I** (−1.40 ppm) has been split into two multiplets centred at 1.79 and 0.17 ppm, consistent with insertion of $CO_2$ into a single Al–C bond. $^{13}C\{^1H\}$ NMR spectroscopy shows a low field peak at 188.8 ppm for the labelled carbon of the metallacycle, which couples to the $CH_2$ methylene peaks ($^1J_{CC}$ = 49 Hz, $^2J_{CC}$ = 6 Hz). IR spectroscopy shows a strong absorption at 1578 cm$^{-1}$, assigned to an exocyclic C=O group. Unfortunately, quenching the reaction with HCl afforded a complex mixture of unidentified products.

Crystals of **1** were isolated from $Et_2O$ as the dimeric species, [{K($Et_2O$)_2}(Al{NON})\{$\kappa^2C,O$-$CH_2CH_2C$(=O)O\}]_2 [**1·(Et₂O)₂**]_2 in which C–C bond formation between $CO_2$ and a carbon of the aluminacyclopropane has occurred (Fig. 2). Each aluminium is spirocyclic, defined by the chelated NON-ligand and a 3-oxido-3-oxopropan-1-ide ligand. The core of the dimer consists of a $K_2O_2$ motif in which the solvated potassium atoms engage in $\mu$-K···O interactions with a neighbouring unit. The endocyclic C–C distances (range: 1.509(5) Å to 1.545(4) Å) indicate single bonds within the metallacycle. However, the endocyclic (1.292(5) Å and 1.302(5) Å) and exocyclic (1.233(4) Å and 1.233(5) Å) C–O distances indicate a degree of delocalization when compared to the expected values for single (1.350 Å) and double (1.201 Å) bonds.[24]
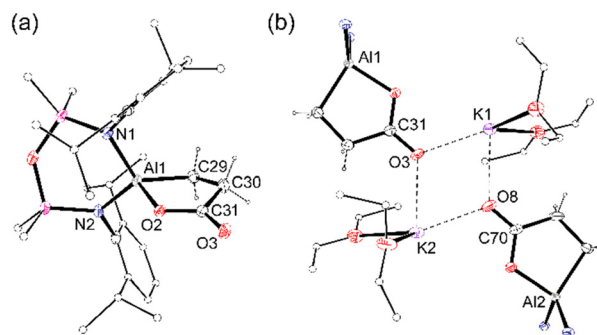


**Fig. 2** (a) Displacement ellipsoid plot (30% probability, H-atoms except $CH_2CH_2$ of metallacycle omitted, C-atoms except at key positions represented as spheres) of one of the [Al(NON){$\kappa^2C,O$–$CH_2CH_2C$(=O)O}]$^-$ anions from [**1·(Et₂O)₂**]_2. Selected bond lengths (Å) and angles (°) {corresponding value from second anion}: Al1–O2 1.8514(19) {1.847(2)}, Al1–C29 1.980(4) {1.984(4)}, C29–C30 1.545(4) {1.517(5)}, C30–C31 1.513(5) {1.509(5)}, C31–O2 1.292(5) {1.302(5)}, C31–O3 1.233(4) {1.233(5)}; C29–Al1–O2 89.77(12) {90.10(13)}, O2–C31–O3 123.1(3) {121.9(3)}, C30–C31–O2 116.2(3) {116.3(3)}, C30–C31–O3 120.7(4) {121.8(4)}. (b) Dimeric core of [**1·(Et₂O)₂**]_2.

The reaction of **I** with diisopropylcarbodiimide (iPrN=C=NiPr) was also performed, affording colourless crystals **2** (Scheme 1). NMR spectroscopic data of **2** resemble those for **1**, with a similar reduction in molecular symmetry evident from new methylene peaks at 2.44 and 0.36 ppm, and a low field resonance in the $^{13}C\{^1H\}$ NMR spectrum at 174.2 ppm for the NCN quaternary carbon. A distinct absorption at 1604 cm$^{-1}$ in the IR spectrum is assigned to a $\nu$(C=N) stretch.

Crystals of **2** suitable for an X-ray diffraction study were grown from the slow evaporation of a toluene/$Et_2O$ solution (Fig. 3). The extended structure shows a 1-D polymer consisting of repeating dimeric [(**2·Et₂O**)(**2**)] units. Each dimer is formed by K···$\pi$(arene) interactions involving the Dipp-substituents of neighbouring units, supplemented by close contacts with
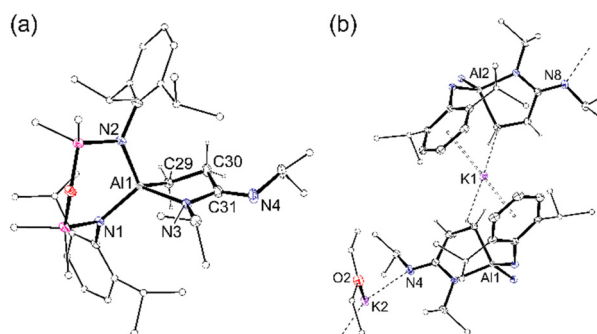


**Fig. 3** (a) Displacement ellipsoid plot (30% probability, H-atoms except $CH_2CH_2$ of metallacycle omitted, C-atoms except at key positions represented as spheres) of one of the [Al(NON){$\kappa^2C,N$-$CH_2CH_2C$(=NiPr)NiPr}]$^-$ anions from [(**2·Et₂O**)(**2**)]. Selected bond lengths (Å) and angles (°) {corresponding value from second anion}: Al1–N3 1.9300(15) {1.9333(15)}, Al1–C29 1.9740(18) {1.9667(18)}, C29–C30 1.533(2) {1.531(2)}, C30–C31 1.534(2) {1.531(2)}, C31–N3 1.370(2) {1.373(2)}, C31–N4 1.305(2) {1.307(2)}; N1–Al–N2 109.91(6) {109.75(6)}, C29–Al1–N3 86.64(7) {88.02(7)}, N3–C31–N4 123.04(17) {122.90(16)}, C30–C31–N3 113.15(15) {113.49(14)}, C30–C31–N4 123.75(17) {123.56(16)}. (b) Dimeric monomer unit of [(**2·Et₂O**)(**2**)]_n.

hydrogen atoms of the metallacyclic $CH_2$ groups. The dimers are linked through solvated $K(Et_2O)$ units that bond to the exocyclic nitrogen atoms of imine groups. As anticipated, the carbodiimide substrate has inserted into one of the alumina-cyclopropane Al–C bonds to afford isopropyl(3-(isopropylimi-no)propan-1-id-3-yl)amide ligands. The C–N bonds in the $AlC_3N$ rings (1.370(2) Å and 1.373(2) Å) are longer than the exocyclic C–N bonds (1.305(2) Å and 1.307(2) Å).

On standing for several days at room temperature, a sample of non-solvated $K[Al(NON)\{CH_2CH_2C(=NiPr)NiPr\}]$ (2) transformed to a new species 3, the $^1H$ NMR of which shows a further reduction in symmetry. Monitoring a sample in benzene showed that this process is complete after 2 days at 80 °C (Fig. S13, ESI†). No such conversion was noted for 1 (100 °C, 5 days). The $^1H$ NMR spectrum of 3 shows that each proton of the $AlC_3N$ metallacycle is in a different environment, with multiplets observed at 2.52, 1.99, 0.12 and −0.46 ppm (1H). Furthermore, the resonances formally associated with the NON-ligand also reflect a reduction in symmetry compared with 2, with four septets for the NON-Dipp substituents, and non-equivalent $SiMe_2$ groups (0.73, 0.36, 0.07 and 0.01 ppm, 3H). These data suggest de-symmetrisation of the NON-ligand, while the retention of a $\nu(C=N)$ stretch at 1608 cm$^{-1}$ indicate that the integrity of the $AlC_3N$ metallacycle is retained.

The slow evaporation of a benzene solution of 3 afforded crystals suitable for X-ray diffraction (Fig. 4). The structure of 3 showed that while the isopropyl(3-(isopropylimino)propan-1-id-3-yl)amide moiety did indeed remain intact at the Al centre, the NON-ligand had undergone a 1,3-silyl retro-Brook rearrangement to afford the corresponding $[NNO]^{2-}$ ligand, $[N(Dipp)SiMe_2N-(Dipp)SiMe_2O]^{2-}$ (Scheme 2). This phenomenon has been studied in the context of $[NON]^{2-}$ dianions, where $Li_2[NON^R]$ was observed to undergo intramolecular rearrangements in THF, with $\tau_{1/2}$ that vary from $5.7 \times 10^1$ s to $1.5 \times 10^8$ s, depending on the R-substituent.[25] However, to the best of our knowledge this process has not been noted for a chelated NON-ligand, in which the $N,N'$-diamido coordination mode is normally considered stable.

The asymmetric unit of 3 consists of $[K(C_6H_6)][Al(NNO)-\{\kappa^2C,N\text{-}CH_2CH_2C(=NiPr)NiPr\}]$ located on an inversion centre, forming a dimeric unit $[3]_2$ linked by contacts between potassium and the exocyclic $N_{imine}$ of the partner complex (K···N4′ = 2.7498(11) Å, Fig. S16, ESI†). The benzene-solvated potassium is bonded to the oxygen of the $[NNO]^{2-}$ ligand, with a K–O distance of 2.6643(9) Å. The bond lengths and angles within the $[CH_2CH_2C(=NiPr)NiPr]^{2-}$ group are essentially the same as those noted in 2. However, switching from an $N,N'$- to an $N,O$-bonding mode for the $[NNO]^{2-}$ ligand reduces the bite angle from 109.91(6)° {109.75(6)°} to 104.83(5)°. Furthermore, the relocation of one of the Dipp-substituents to the rear of the ligand significantly reduces the steric demand of the ligand at the aluminium centre. This was confirmed quantitatively using % volume buried measurements ($\%V_{Bur}$),[26] performed on the 'Al(NON)' and 'Al(NNO)' fragments (Fig. 4b), which generate values of 72.7% for $[NON]^{2-}$ and 63.3% for $[NNO]^{2-}$.

The mechanism for the rearrangement of 2 to 3 was examined using DFT (Fig. 5. See ESI† for full computational details).
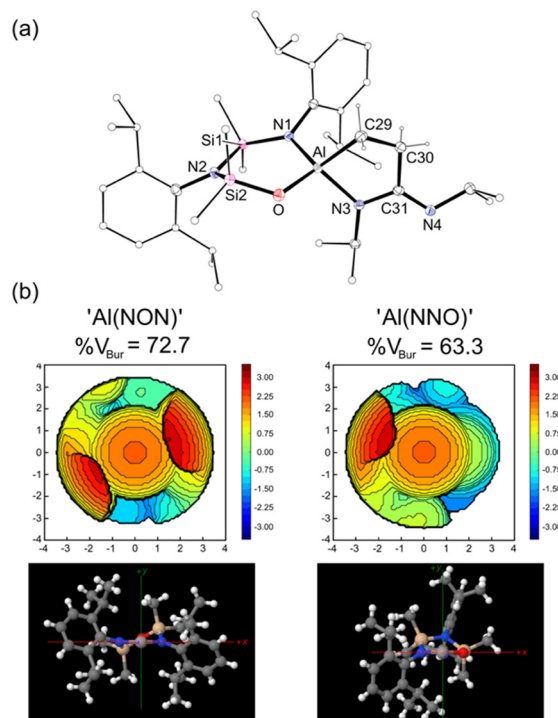


Fig. 4 (a) Displacement ellipsoid plot ('−x, 1 − y, 1 − z, 30% probability, H-atoms except $CH_2CH_2$ of metallacycle omitted, C-atoms except at key positions represented as spheres) of the $[Al(NNO)\{\kappa^2C,N\text{-}CH_2CH_2C(=NiPr)NiPr\}]^-$ anion from $[3]_2$. Selected bond lengths (Å) and angles (°): Al–O 1.7694(10), Al–N1 1.8789(11), Al–C29 1.9739(14), Al–N3 1.9041(11), C29–C30 1.538(2), C30–C31 1.5285(18), C31–N3 1.3722(17), C31–N4 1.3019(18), O–Al–N1 104.83(5), Al–O–Si2 122.75(6), C29–Al–N3 88.45(5), N3–C31–N4 122.99(12), C30–C31–N3 112.99(11), C30–C31–N4 123.99(12). (b) Topographic steric maps of 'Al(NON)' and 'Al(NNO)' fragments (3.5 Å radius around Al, Bondi radii scaled by 1.17).
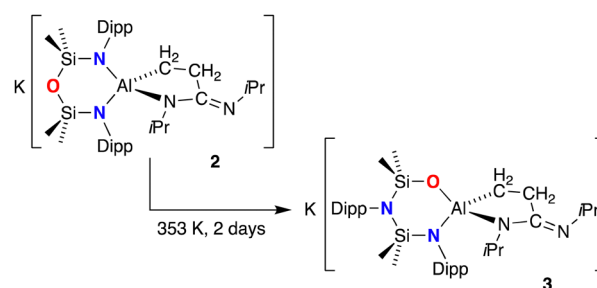


Scheme 2 Conversion of (non-solvated) 2 to 3.

The starting point for the calculations was the non-solvated monomer $K[Al(NON)\{CH_2CH_2C(=NiPr)NiPr\}]$ ($2^{DFT}$), in which the potassium is $\eta^6$-bound to a Dipp substituent with additional K···H support from a methylene hydrogen atom. The first transition-state $TS(2^{DFT}\text{-}A)^{\ddagger}$ was located at 15.8 kcal mol$^{-1}$ and involves Al–N2 dissociation, leading to the four-membered aluminacycle A where the formally NON-ligand is coordinated through the remaining nitrogen atom (N1) and the backbone oxygen. Although the oxygen-atom is commonly involved in tridentate bonding of the NON-ligand, examples of exclusively $\kappa N,O$-bonded species are restricted to potassium[27] and magnesium.[28] From A, after rotation
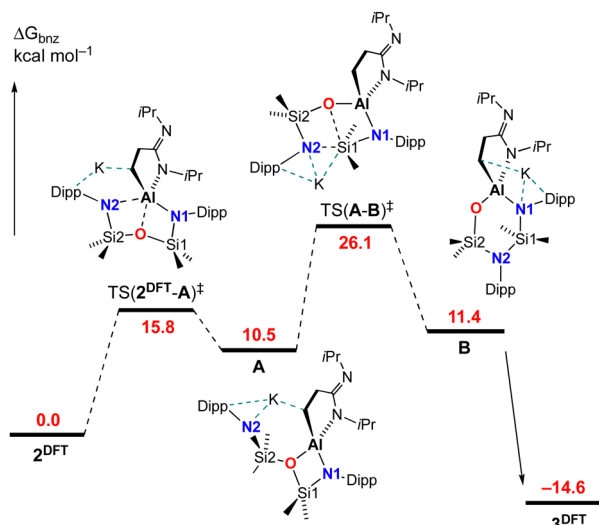
**Fig. 5** Computed free energy profile (BP86-D3BJ(PCM=$C_6H_6$)/BS2//BP86/BS1 in kcal mol$^{-1}$) for 1,3-silyl retro-Brook rearrangement converting K[Al(NON){CH$_2$CH$_2$C(=NiPr)NiPr}] (**2$^{DFT}$**) to K[Al(NNO){CH$_2$CH$_2$C(=NiPr)NiPr}] (**3$^{DFT}$**).

about O–Si2, bond formation between the dissociated N2 nitrogen atom and Si1 occurs in transition state TS(**A–B**)$^{\ddagger}$, which is rate determining with a barrier of 15.6 kcal mol$^{-1}$. This leads to a second intermediate **B** in which Si1–O bond cleavage has occurred, and an NNO-coordination mode has been achieved. The reaction pathway from **B** to the computed monomer K[Al(NNO){CH$_2$CH$_2$C(=NiPr)NiPr}] **3$^{DFT}$**, with an energy of −14.6 kcal mol$^{-1}$, has also been identified (Fig. S18, ESI†). It plots the migration of the K-atom from the N1-Dipp group to oxygen, whilst maintaining contacts to the 'CN$_2$' component of the [{CH$_2$CH$_2$C(=NiPr)NiPr}]-ligand.

In summary we have shown that the aluminacyclopropane anion [Al(NON)(η-C$_2$H$_4$)]$^-$ reacts with CO$_2$ and iPrNCNiPr to form cyclo-AlC$_3$X (X = O or N{R}) products *via* C–C bond formation. Upon heating an intramolecular retro-Brook rearrangement of the chelating NON-ligand occurs at aluminium. DFT calculations identified a key intermediate that involves a bimetallic Al/K species where the chelating NON-diamide has adopted a ring-contracted *N,O*-coordination. The results of equivalent insertion/NON → NNO rearrangements during the reaction of **I** with other unsaturated substrates will be reported in a subsequent manuscript.

## Conflicts of interest

There are no conflicts to declare.

## References

1 (*a*) C. Weetman and S. Inoue, *ChemCatChem*, 2018, **10**, 4213–4228; (*b*) P. P. Power, *Nature*, 2010, **463**, 171–177.
2 K. Hobson, C. J. Carmalt and C. Bakewell, *Chem. Sci.*, 2020, **11**, 6942–6956.
3 (*a*) M. P. Coles and M. J. Evans, *Chem. Commun.*, 2023, **59**, 503–519; (*b*) J. Hicks, P. Vasko, J. M. Goicoechea and S. Aldridge, *Angew. Chem., Int. Ed.*, 2021, **60**, 1702–1713.
4 https://www.statista.com/statistics/1245262/acrylic-acid-market-volume-worldwide/. Retrieved Nov. 08, 2023.
5 A. Brennführer, H. Neumann and M. Beller, *ChemCatChem*, 2009, **1**, 28–41.
6 M. M. Lin, *Appl. Catal., A*, 2001, **207**, 1–16.
7 (*a*) T. Schaub, A. S. K. Hashmi and R. A. Paciello, *J. Org. Chem.*, 2019, **84**, 4604–4614; (*b*) X. Wang, H. Wang and Y. Sun, *Chemistry*, 2017, **3**, 211–228; (*c*) M. Hollering, B. Dutta and F. E. Kühn, *Coord. Chem. Rev.*, 2016, **309**, 51–67; (*d*) M. Limbach, *Adv. Organomet. Chem.*, 2015, **63**, 175–202.
8 P. N. Plessow, A. Schäfer, M. Limbach and P. Hofmann, *Organometallics*, 2014, **33**, 3657–3668.
9 S. A. Cohen and J. E. Bercaw, *Organometallics*, 1985, **4**, 1006–1014.
10 H. G. Alt and C. E. Denner, *J. Organomet. Chem.*, 1990, **390**, 53–60.
11 B. Hessen, A. Meetsma, F. Van Bolhuis, J. H. Teuben, G. Helgesson and S. Jagner, *Organometallics*, 1990, **9**, 1925–1936.
12 (*a*) R. Alvarez, E. Carmona, A. Galindo, E. Gutierrez, J. M. Marin, A. Monge, M. L. Poveda, C. Ruiz and J. M. Savariault, *Organometallics*, 1989, **8**, 2430–2439; (*b*) R. Alvarez, E. Carmona, D. J. Cole-Hamilton, A. Galindo, E. Gutierrez-Puebla, A. Monge, M. L. Poveda and C. Ruiz, *J. Am. Chem. Soc.*, 1985, **107**, 5529–5531.
13 (*a*) T. T. Adamson, S. P. Kelley and W. H. Bernskoetter, *Organometallics*, 2020, **39**, 3562–3571; (*b*) S. M. Rummelt, H. Zhong, I. Korobkov and P. J. Chirik, *J. Am. Chem. Soc.*, 2018, **140**, 11589–11593; (*c*) H. Hoberg, K. Jenni, K. Angermund and C. Krüger, *Angew. Chem., Int. Ed. Engl.*, 1987, **26**, 153–155.
14 T. Ito, K. Takahashi and N. Iwasawa, *Organometallics*, 2019, **38**, 205–209.
15 (*a*) S. Takegasa, M. M. Lee, K. Tokuhiro, R. Nakano and M. Yamashita, *Chem. – Eur. J.*, 2022, **28**, e202201870; (*b*) M. Aresta and E. Quaranta, *J. Organomet. Chem.*, 1993, **463**, 215–221.
16 (*a*) K. Takahashi, K. Cho, A. Iwai, T. Ito and N. Iwasawa, *Chem. – Eur. J.*, 2019, **25**, 13504–13508; (*b*) I. Knopf, D. Tofan, D. Beetstra, A. Al-Nezari, K. Al-Bahily and C. C. Cummins, *Chem. Sci.*, 2017, **8**, 1463–1468; (*c*) N. Huguet, I. Jevtovikj, A. Gordillo, M. L. Lejkowski, R. Lindner, M. Bru, A. Y. Khalimon, F. Rominger, S. A. Schunk, P. Hofmann and M. Limbach, *Chem. – Eur. J.*, 2014, **20**, 16858–16862; (*d*) C. Hendriksen, E. A. Pidko, G. Yang, B. Schäffner and D. Vogt, *Chem. – Eur. J.*, 2014, **20**, 12037–12040; (*e*) M. L. Lejkowski, R. Lindner, T. Kageyama, G. É. Bódizs, P. N. Plessow, I. B. Müller, A. Schäfer, F. Rominger, P. Hofmann, C. Futter, S. A. Schunk and M. Limbach, *Chem. – Eur. J.*, 2012, **18**, 14017–14025; (*f*) H. Hoberg, Y. Peres, C. Krüger and Y.-H. Tsay, *Angew. Chem., Int. Ed. Engl.*, 1987, **26**, 771–773.
17 S. C. E. Stieber, N. Huguet, T. Kageyama, I. Jevtovikj, P. Ariyananda, A. Gordillo, S. A. Schunk, F. Rominger, P. Hofmann and M. Limbach, *Chem. Commun.*, 2015, **51**, 10907–10909.
18 V. N. Solov'ev, E. V. Polikarpov, A. V. Nemukhin and G. B. Sergeev, *J. Phys. Chem. A*, 1999, **103**, 6721–6725.
19 (*a*) C. Bakewell, A. J. P. White and M. R. Crimmin, *Angew. Chem., Int. Ed.*, 2018, **57**, 6638–6642; (*b*) C. Bakewell, A. J. P. White and M. R. Crimmin, *Chem. Sci.*, 2019, **10**, 2452–2458.
20 R. Y. Kong and M. R. Crimmin, *Chem. Commun.*, 2019, **55**, 6181–6184.
21 (*a*) J. Hicks, P. Vasko, J. M. Goicoechea and S. Aldridge, *J. Am. Chem. Soc.*, 2019, **141**, 11000–11003; (*b*) K. Sugita, R. Nakano and M. Yamashita, *Chem. – Eur. J.*, 2020, **26**, 2174–2177.
22 R. J. Schwamm, M. D. Anker, M. Lein and M. P. Coles, *Angew. Chem., Int. Ed.*, 2019, **58**, 1489–1493.
23 M. J. Evans, S. E. Neale, M. D. Anker, C. L. McMullin and M. P. Coles, *Angew. Chem., Int. Ed.*, 2022, **61**, e202117396.
24 F. H. Allen, O. Kennard, D. G. Watson, L. Brammer, A. G. Orpen and R. Taylor, *J. Chem. Soc., Perkin Trans. 2*, 1987, S1–S19.
25 (*a*) F. Haftbaradaran, G. Mund, R. J. Batchelor, J. F. Britten and D. B. Leznoff, *Dalton Trans.*, 2005, 2343–2345; (*b*) F. Haftbaradaran, A. M. Kuchison, M. J. Katz, G. Schatte and D. B. Leznoff, *Inorg. Chem.*, 2008, **47**, 812–822.
26 L. Falivene, Z. Cao, A. Petta, L. Serra, A. Poater, R. Oliva, V. Scarano and L. Cavallo, *Nat. Chem.*, 2019, **11**, 872–879.
27 M. D. Anker, M. Lein and M. P. Coles, *Chem. Sci.*, 2019, **10**, 1212–1218.
28 R. J. Schwamm and M. P. Coles, *Chem. – Eur. J.*, 2019, **25**, 14183–14191.